

Environmentally Selected WIMP Dark Matter with High-Scale Supersymmetry Breaking

Gilly Elor^a, Hock-Seng Goh^a, Lawrence J. Hall^{a,b}, Piyush Kumar^a, and Yasunori Nomura^{a,b}

^a *Berkeley Center for Theoretical Physics,
and Theoretical Physics Group, Lawrence Berkeley National Laboratory
University of California, Berkeley, CA 94720, USA*

^b *Institute for the Physics and Mathematics of the Universe,
University of Tokyo, Kashiwa 277-8568, Japan*

Abstract

We explore the possibility that both the weak scale and the thermal relic dark matter abundance are environmentally selected in a multiverse. An underlying supersymmetric theory containing the states of the MSSM and singlets, with supersymmetry and R symmetry broken at unified scales, has just two realistic low energy effective theories. One theory, $(\text{SM} + \tilde{w})$, is the Standard Model augmented only by the wino, having a mass near 3 TeV, and has a Higgs boson mass in the range of (127 – 142) GeV. The other theory, $(\text{SM} + \tilde{h}/\tilde{s})$, has Higgsinos and a singlino added to the Standard Model. The Higgs boson mass depends on the single new Yukawa coupling of the theory, y , and is near 141 GeV for small y but grows to be as large as 210 GeV as this new coupling approaches strong coupling at high energies. Much of the parameter space of this theory will be probed by direct detection searches for dark matter that push two orders of magnitude below the present bounds; furthermore, the dark matter mass and cross section on nucleons are correlated with the Higgs boson mass. The indirect detection signal of monochromatic photons from the galactic center is computed, and the range of parameters that may be accessible to LHC searches for trilepton events is explored. Taking a broader view, allowing the possibility of R symmetry protection to the TeV scale or axion dark matter, we find four more theories: $(\text{SM} + \text{axion})$, two versions of Split Supersymmetry, and the E-MSSM, where a little supersymmetric hierarchy is predicted. The special Higgs mass value of (141 ± 2) GeV appears in symmetry limits of three of the six theories, $(\text{SM} + \text{axion})$, $(\text{SM} + \tilde{w})$ and $(\text{SM} + \tilde{h}/\tilde{s})$, motivating a comparison of other signals of these three theories.

Contents

1	Introduction and Framework	1
2	A Model with Comparable Higgsino and Singlino Masses	4
3	The Higgs Boson Mass	5
4	Dark Matter	9
4.1	Relic abundance	9
4.2	Direct detection	10
5	Experimental Signals	12
5.1	Higgs mass measurements at the Tevatron and the LHC	12
5.2	LHC signals	12
5.3	Direct detection of dark matter	15
5.4	Indirect detection of dark matter	17
6	SM + Wino as an Effective Theory below the Unified Scale	19
7	Discussion and Conclusions	20

1 Introduction and Framework

The extremely small value of the cosmological constant—at least 120 orders below its natural value—has resisted explanation from symmetry principles. Furthermore, since the discovery of dark energy, with $w = -1.0 \pm 0.1$ [1, 2], there appears to be a second part to the cosmological constant problem: why does it take the observed value, which is close to the matter density at the present epoch? Environmental arguments solve both pieces of the puzzle, at least at the order of magnitude level [3], motivating searches for further evidence of environmental selection. While there are symmetry arguments for understanding why the weak scale is 16 orders of magnitude less than its natural value in the Standard Model (SM), no direct experimental evidence for any such symmetry extension of the SM has been found so far in the preliminary exploration of the weak scale. On the other hand, it is intriguing that if the weak scale were increased by a factor of 2, the SM would not yield any complex stable nuclei [4], suggesting that the weak scale may also be selected environmentally.

Such arguments from environmental selection only make sense if the underlying theory of nature has a vast landscape of vacua, allowing a fine scanning of parameters. The realization that string theory, with a compact manifold of extra dimensions, may yield such a landscape [5] strengthens the motivation for seeking further evidence for environmental selection on a multiverse. String theory requires supersymmetry; however, if the weak scale is environmental, it is reasonable to consider that the scale of supersymmetry breaking is high, i.e. close to the string scale rather than to the weak scale. Hence, in this paper we explore the case of very high scale supersymmetry breaking, with the physics of electroweak symmetry breaking described purely by the SM Higgs boson.

This appears to leave no room for weakly interacting massive particle (WIMP) dark matter, since no new stable particles have masses that are logically connected to weak symmetry breaking. Instead, we

assume that there is an environmental requirement for dark matter. This assumption now plays a central role, since it determines the properties of the dark matter and the size of the cosmological constant. In particular, we assume that dark matter arises from a conventional freezeout process through interactions with couplings that are order unity. The environmentally allowed range of the dark matter density is unknown [6], but we do not need to assume that it is very narrow. Even if the range spans several orders of magnitude, the selection process leads to dark matter particles having masses within an order of magnitude or two of the weak scale. However, we stress that the connection between the dark matter mass, m_{DM} , and the weak scale, v , is now purely coincidental.

Our framework for high scale supersymmetry breaking, with independent environmental selections of the weak scale and dark matter, is as follows. The scale of supersymmetry breaking in the SM sector, \tilde{m} , is taken close to the cutoff of the effective field theory at the string scale, M_* . At \tilde{m} the theory is taken to have the states of the Minimal Supersymmetric Standard Model (MSSM) together with gauge singlet chiral multiplets S . The environmental selection for dark matter requires some states beyond those of the SM to be much lighter than \tilde{m} . As supersymmetry breaks near M_* , the R symmetry $U(1)_R$ must also be broken at a very high scale to cancel the cosmological constant. It is then likely that R breaking is transmitted to the MSSM sector without large suppression, making the gauginos very heavy. It is possible that such a strong transmission is avoided, leading to the Split Supersymmetry theory [7]. In this case, environmental selection of dark matter acting on the symmetry breaking parameter of a particular R symmetry can protect all fermionic superpartners to near the weak scale.

In this paper we explore the simple possibility that R breaking in the MSSM sector is unsuppressed. In this case, what is the origin of the small weak-scale mass needed for WIMP dark matter? Environmental selection could lead either to a cancellation of terms in the mass of some particle, or to a theory with an approximate symmetry that protects some light states. In the former case dark matter would be fermionic, since for fermions the cancellation is linear in the mass, while for scalars it is quadratic. Also, the dark matter sector would contain just a single fermion, since there is a cost for each cancellation. Since pure Higgsino dark matter is observationally excluded and a pure singlino does not freeze-out at the weak scale, in our framework the only possibility with mass cancellation is pure wino dark matter, \tilde{w} . If the mass of the dark matter sector is protected by an approximate symmetry, there is again a unique possibility. Since supersymmetry is broken at the high scale, the approximate symmetry cannot keep scalars light. Furthermore, since the approximate symmetry must be a non- R symmetry it cannot protect gauginos either, so that the only states that it can protect are the Higgsinos and singlinos, \tilde{h}_u , \tilde{h}_d and \tilde{s} . Realistic WIMP dark matter requires that all three states are involved.

Thus with high scale breaking of the R symmetry, we are led to two possibilities for environmental WIMP dark matter: selection of a small wino mass, or selection of an approximate symmetry that protects the Higgsinos and singlino. We do not know which of these possibilities has a higher probability in the multiverse. In Figure 1, we illustrate how accurately gauge coupling unification occurs in these two theories compared to the SM. The quantity $\delta(E)$ is a measure of the size of the threshold corrections needed to unify the couplings at scale E . In all three theories unification occurs near 10^{14} GeV. The SM and the SM + \tilde{w} theory require comparable threshold corrections of (5 – 6)%, while SM + \tilde{h}/\tilde{s} yields gauge coupling unification that is almost as precise as in the MSSM [8, 9]. Since gauge coupling unification occurs at a scale $M_u \sim 10^{14}$ GeV, suppression of gauge-mediated proton decay suggests unification into higher dimensions [10], which can bring gauge coupling unification for the SM + \tilde{h}/\tilde{s} theory to an even higher level of precision [11, 9]. We study both these theories in this paper; various aspects of the SM + \tilde{h}/\tilde{s} theory and its signals are explored in sections 2 – 5, and wino dark matter in

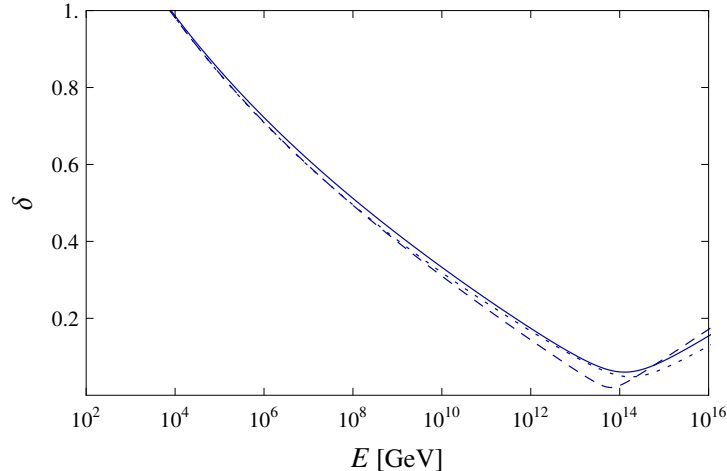


Figure 1: The threshold correction δ required for gauge coupling unification at energy E in the SM (solid), in SM + \tilde{h}/\tilde{s} (dashed), and in SM + \tilde{w} (dotted). All three theories unify near 10^{14} GeV, with varying levels of precision. Here $\delta \equiv \sqrt{(g_1^2 - \bar{g}^2)^2 + (g_2^2 - \bar{g}^2)^2 + (g_3^2 - \bar{g}^2)^2}/\bar{g}^2$, where $\bar{g}^2 \equiv (g_1^2 + g_2^2 + g_3^2)/3$.

the SM + \tilde{w} theory is examined in section 6.

In previous studies of mixed doublet/singlet fermion dark matter inspired by an environmental weak scale, the theory studied was the most general allowed for the doublet/singlet system [8, 9]. The Higgsino/singlino dark matter theory studied in this paper is a new version, which emerges from the supersymmetric framework described above and keeps the successful features of gauge coupling unification and WIMP dark matter. Supersymmetry plays a key role since it leads to a high precision prediction for the Higgs boson mass, and it restricts the form of the Yukawa couplings to the new states. In this SM + \tilde{h}/\tilde{s} theory, the Higgsino mass, μ , transforms non-trivially under some approximate symmetry G and, since G is not an R symmetry, the Higgs-boson mass mixing parameter, B_μ , must also be suppressed: $\mu \sim \epsilon \tilde{m}$ and $B_\mu \sim \epsilon \tilde{m}^2$, where ϵ is a small symmetry breaking parameter. This implies that environmental selection on the Higgs mass matrix to obtain a low weak scale leads to the light Higgs boson being $h \sim h_u + \epsilon h_d$ or $h \sim h_d + \epsilon h_u$, with $\epsilon \sim m_{\text{DM}}/\tilde{m} \sim O(10^{-12} - 10^{-11})$. The heavy top quark prefers the former case, so that quark and charged lepton masses arise from

$$\mathcal{L} \sim [QUH_u]_{\theta^2} + \frac{1}{M_*^2} [(QD + LE)H_u^\dagger X^\dagger]_{\theta^4} + \text{h.c.}, \quad (1)$$

where Q, U, D, L, E are the quark and lepton superfields, H_u a Higgs superfield and X a superfield that leads to supersymmetry breaking, $\langle X \rangle = \theta^2 F_X$ with $F_X \sim \tilde{m} M_*$. Hence the b quark and τ lepton masses are moderately suppressed relative to the t quark mass by supersymmetry breaking, $m_{b,\tau}/m_t \sim \tilde{m}/M_*$.

As in the MSSM, supersymmetry imposes a boundary condition on the Higgs quartic coupling, but with two important differences. First, the boundary condition applies near the unified scale rather than near the weak scale and, as we will see in section 3, this has crucial consequences for the prediction of the Higgs boson mass. Secondly, since $\tan \beta \sim 1/\epsilon$, the boundary condition becomes independent of $\tan \beta$

$$\lambda(\tilde{m}) = \frac{g^2(\tilde{m}) + g'^2(\tilde{m})}{8} (1 + \delta), \quad (2)$$

	Q	U	D	L	E	H_u	H_d	S	ϵ
Z_3	q	$-1 - q$	$1 - q$	l	$1 - l$	1	1	1	1

Table 1: The charge assignment under $G = Z_3$, where q and l are arbitrary numbers.

where δ results from threshold corrections, for example, from integrating out superpartners such as the top squarks.

Since \tilde{s} is lighter than \tilde{m} , the superfield S must also transform non-trivially under G . This removes interactions that transform linearly in S , such as $[SX^\dagger X]_{\theta^4}$. The G charges must allow $[SH_u H_d]_{\theta^2}$, since otherwise \tilde{s} would not interact in the low energy theory, preventing acceptable dark matter. Hence the theory below \tilde{m} is described by

$$\mathcal{L} = \mathcal{L}_{\text{SM}}(q, u, d, l, e, h) + \left\{ \mu \tilde{h}_u \tilde{h}_d + \frac{m}{2} \tilde{s}^2 + y \tilde{h}_d \tilde{s} h + \text{h.c.} \right\}, \quad (3)$$

where we drop higher dimension interactions and dimensionless interactions suppressed by powers of ϵ . Supersymmetry together with G removes the gauge invariant interaction $\tilde{h}_u \tilde{s} h^\dagger$, so that there are just three new parameters: μ , m and y . Since the quartic coupling is predicted in Eq. (2), the theory has just two more free parameters than the SM.

In the next section we present a particular realization of our SM + \tilde{h}/\tilde{s} theory, with $G = Z_3$. In section 3 we present the Higgs mass prediction, finding that it is extremely insensitive to y for $y(\tilde{m}) \lesssim 0.4$. The constraints on the parameter space imposed by the requirement of dark matter are studied in section 4. In section 5 we study experimental signals from hadron colliders and from the direct and indirect detection of dark matter. In section 6 we study wino dark matter in the SM + \tilde{w} theory. Discussion and conclusions are given in section 7.

2 A Model with Comparable Higgsino and Singlino Masses

In this section we present a model that realizes the framework where dark matter is protected by a chiral symmetry G . We consider that the theory above \tilde{m} is the MSSM with a singlet superfield S . We also assume that the theory possesses usual R parity, under which S is even, and that supersymmetry breaking does not violate G so that the protection of dark matter persists below \tilde{m} . This implies that the supersymmetry breaking field X is neutral under G .

We consider that the Higgsinos and singlino obtain masses in the same way via a single symmetry breaking spurion ϵ : $\mathcal{L} \sim [\epsilon M_* H_u H_d + \epsilon M_* S^2]_{\theta^2}$. We also require that the Yukawa coupling $[SH_u H_d]_{\theta^2}$ exists, allowing the Higgsinos to mix with the singlino. We then find, using the freedom of redefining G charges through hypercharge, that $G = Z_3$ is the unique possibility under which H_u , H_d , and S , as well as the symmetry breaking spurion ϵ , all carry a charge of +1. The existence of the Yukawa couplings of Eq. (1) then implies that the charge of QU , QD , and LE are -1 , $+1$, and $+1$, respectively. The most general charge assignment under G is thus given as in Table 1.

Because of supersymmetry breaking, all the gaugino and scalar fields decouple at the scale \tilde{m} , except for a single Higgs doublet required by environmental selection. All the supersymmetry breaking parameters are of order \tilde{m} , except for the holomorphic squared masses for $H_{u,d}$ and S (and a linear term for S ;

see below), which are suppressed by ϵ . This implies that the Higgs mass-squared matrix takes the form

$$\mathcal{L} \sim \begin{pmatrix} h_u^\dagger & h_d \end{pmatrix} \begin{pmatrix} \tilde{m}_2^2 & \epsilon \tilde{m}_3^2 \\ \epsilon \tilde{m}_3^2 & \tilde{m}_1^2 \end{pmatrix} \begin{pmatrix} h_u \\ h_d^\dagger \end{pmatrix}, \quad (4)$$

where $\tilde{m}_{1,2,3}^2$ are typically of order \tilde{m}^2 and scan independently in the multiverse. Given that environmental selection requires one eigenvalue of this matrix to be of order v^2 , what is the most probable linear combination left at low energies? We find that the low energy doublet, h , is mostly h_u (or h_d) with only a tiny, $O(\epsilon)$ mixture of h_d (h_u). Motivated by the large top quark mass, we consider

$$h \sim h_u + \epsilon h_d, \quad (5)$$

which corresponds to the case where the environmental requirements selects $\tilde{m}_2^2 \sim O(\epsilon^2 \tilde{m}^2)$ and $\tilde{m}_1^2 \sim \tilde{m}_3^2 \sim O(\tilde{m}^2)$. This implies that the low-energy SM Higgs doublet is essentially h_u in this model.

The charge assignment of Table 1 allows operators such as $[\epsilon^2 M_*^2 S]_{\theta^2}$, $[S^3]_{\theta^2}$, and $[\epsilon X^\dagger X S^\dagger / M_*]_{\theta^4}$. In particular, the last operator induces a vacuum expectation value of the S field, of order $\langle S \rangle \sim \epsilon M_*$. This is, however, not a problem, and the low-energy Lagrangian still takes the form of Eq. (3), with $\mu \sim m \sim O(\epsilon M_*)$. The environmental requirement for dark matter will then select $\epsilon M_* \sim O(100 \text{ GeV} - \text{TeV})$. The Yukawa coupling y is not suppressed by ϵ and is generically expected to be of order unity.

The other possible Yukawa coupling $\tilde{h}_u \tilde{s} h^\dagger$, allowed by gauge invariance, is suppressed by ϵ . This has an important consequence that the new fermionic sector at the weak scale, $\tilde{h}_{u,d}$ and \tilde{s} , does not give any appreciable electric dipole moments for the SM particles, since all the phases of μ , m and y can be absorbed by field redefinitions of $\tilde{h}_{u,d}$ and \tilde{s} . An observation of nonzero electric dipole moments for the electron, neutron or atoms in future experiments would therefore exclude the model.

Neutrino masses can be obtained by choosing $l = -1 \pmod{3}$ through operators $[(LH_u)^2 / M_*]_{\theta^2}$. Since M_* is expected not far from the scale of gauge coupling unification, $\approx 10^{14} \text{ GeV}$, this gives the desired size for the masses. Alternatively, we can introduce right-handed neutrino superfields with the charge $N(-1-l)$ and the Yukawa couplings $[LNH_u]_{\theta^2}$. For $l = -1 \pmod{3}$, this allows the conventional seesaw mechanism. For $l+1 \neq 0, \pm 1/2, \pm 1, 3/2$, the Majorana masses for N are forbidden; but Dirac neutrino masses of the right size can still be obtained if we take the Yukawa couplings to be of $O(10^{-13} - 10^{-12})$.

The choice for q is arbitrary. For $3q+l \neq 0 \pmod{3}$, proton decay is (almost) completely suppressed. This does not contradict gauge coupling unification, if grand unification is realized in higher dimensions and matter fields propagate in the bulk [10].

3 The Higgs Boson Mass

The supersymmetric boundary condition of Eq. (2) on the Higgs quartic coupling λ , leads to a Higgs mass prediction in the SM + \tilde{h}/\tilde{s} theory described by Eq. (3). In this section we compute the Higgs boson mass, paying attention to a variety of uncertainties.

Gauge coupling unification occurs with high precision in the SM + \tilde{h}/\tilde{s} theory, determining the scale of unification M_u to be within an order of magnitude of 10^{14} GeV . This scale may be closely related to a compactification scale of the compact manifold of string theory, and may not be far below the field theory cutoff scale M_* . Since we are taking the supersymmetry breaking scale \tilde{m} to be very high, could it be close to M_* in such a way that the supersymmetric boundary condition on λ is destroyed? Naively the supersymmetry breaking corrections to the boundary condition are $\delta\lambda \sim (\tilde{m}/M_*)^2$. In fact, in many

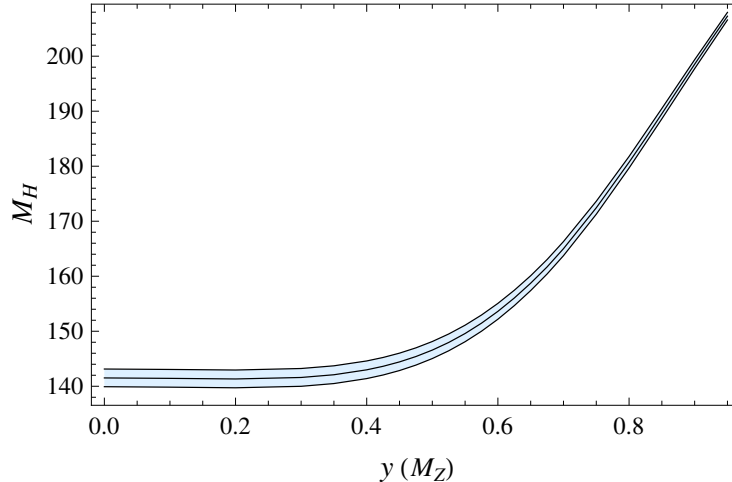


Figure 2: The Higgs mass prediction in the SM + \tilde{h}/\tilde{s} theory as a function of $y(M_Z)$. The curve represents the prediction for $m_t = 173.1$ GeV, with the shaded band corresponding to the uncertainty that arises from the experimental error in the top quark mass of ± 1.3 GeV. The supersymmetry breaking scale and QCD coupling are fixed at $\tilde{m} = 10^{14}$ GeV and $\alpha_s(M_Z) = 0.1176$, respectively.

theories the corrections are suppressed, even as \tilde{m} approaches M_* [12]. This is because the large value of the Planck scale, $M_{\text{Pl}} \gg M_*$, implies a large volume for the compact manifold. For example, suppose that supersymmetry breaking is localized in the bulk and separated from the location of the Higgs multiplet. In this case, supersymmetry breaking is transmitted non-locally; gravitational mediation is suppressed by the volume of the bulk, while gauge mediations is loop suppressed. Alternatively, supersymmetry breaking may occur through a nontrivial boundary condition in the manifold. The corrections to the Higgs quartic coupling are also volume suppressed in this case.

Our basic result for the Higgs boson mass is shown in Figure 2 where, motivated by the scale of gauge coupling unification, we have taken $\tilde{m} = 10^{14}$ GeV. We have assumed that states associated with unification are above \tilde{m} , so that the theory below \tilde{m} is the SM + \tilde{h}/\tilde{s} theory with the single unknown parameter y . The Higgs mass prediction is shown for the full range of $y(M_Z)$ that maintains y perturbative to \tilde{m} . All figures and analytical results are obtained using two-loop renormalization group (RG) scaling of all couplings from \tilde{m} to the weak scale, together with one-loop threshold corrections at the weak scale, including the one-loop effective potential for the Higgs field. In addition, we include the two- and three-loop QCD threshold corrections in converting the top-quark pole mass to the $\overline{\text{MS}}$ top Yukawa coupling, since they are anomalously large.

The prediction of Figure 2 is shown as a shaded band that has a width corresponding to the present experimental error in the top quark mass, $m_t = (173.1 \pm 1.3)$ GeV [13]. The QCD coupling is fixed at $\alpha_s(M_Z) = 0.1176$ [14]; the uncertainty in the Higgs boson mass arising from the experimental error, ± 0.002 , of $\alpha_s(M_Z)$ is smaller than that from the m_t error by about a factor of 2. In the “small y ” region, $y \lesssim 0.4$, the prediction is almost independent of y : $M_H \simeq (141 - 142)$ GeV, with an error of about 1.5% arising from the m_t and α_s uncertainties. In this region the prediction is very close to the case that only the SM survives below \tilde{m} [12]; the coupling y has a negligible effect and the Higgsino contributions to the gauge beta functions raise the Higgs mass by only about half a GeV. In the “large y ” region, $y \gtrsim 0.7$, the Higgs mass prediction rises linearly with $y(M_Z)$, reaching a maximum value of ≈ 210 GeV. Much

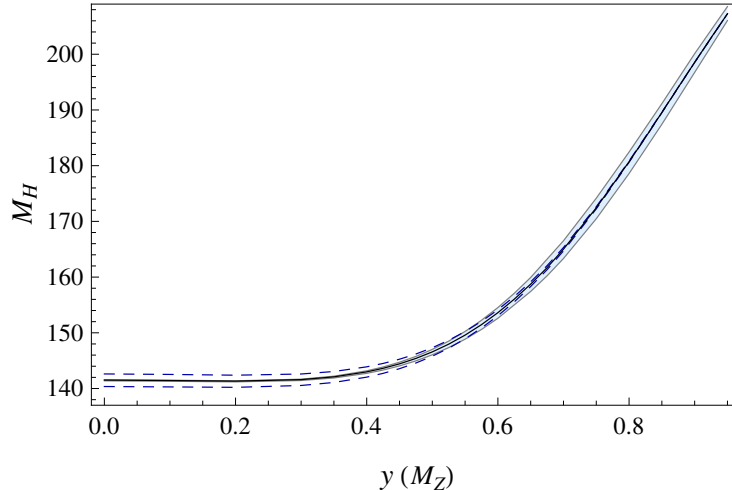


Figure 3: The sensitivity of the Higgs mass prediction to \tilde{m} and δ in the SM + \tilde{h}/\tilde{s} theory. The shaded band corresponds to the variation of \tilde{m} by an order of magnitude above and below 10^{14} GeV. The dashed lines show the predictions for $\delta = \pm 0.1$, with \tilde{m} fixed to 10^{14} GeV.

of the RG scaling of the quartic coupling now arises from y , reducing the sensitivity to the top Yukawa coupling, as shown by the narrowing of the shaded band as y increases.

Two important sources of corrections to the prediction arise from threshold corrections to the supersymmetric boundary condition, δ in Eq. (2), and the choice of matching scale, \tilde{m} . In fact, one needs a prescription to determine how much of the threshold corrections are absorbed into the matching scale. We absorb all leading-log threshold corrections into the matching scale, so that δ contains only the non-log terms.

The sensitivity of the Higgs mass prediction to the scale \tilde{m} is shown by the shaded band in Figure 3, where \tilde{m} is varied by an order of magnitude above and below 10^{14} GeV. Including all leading-log threshold corrections from an arbitrary superpartner spectrum in our theory, we find that just a few of the superpartner masses dominate the matching scale

$$\tilde{m} \simeq \begin{cases} m_\lambda^{1.6}/m_{\tilde{t}}^{0.6} & \text{for small } y \\ \sqrt{m_s m_H} & \text{for large } y \end{cases}, \quad (6)$$

where m_λ and $m_{\tilde{t}}$ are the gaugino and top squark masses, while m_s and m_H are the masses of the scalar superpartner of \tilde{s} and the heavy Higgs boson, respectively. We ignore non-degeneracies amongst the gaugino masses at this high scale. Although \tilde{m} does not coincide with any particular superparticle mass, it is in the vicinity of $m_\lambda, m_{\tilde{t}}, m_s$, and m_H . In the small y region the sensitivity of the Higgs mass to \tilde{m} is extremely small, due to a combination of the convergence property discussed below and the flatness of the trajectories of λ at high scales. This sensitivity to \tilde{m} grows with y , as the trajectories of λ at high scales become less flat, so that by $y = 0.8$, varying \tilde{m} by an order of magnitude causes a 2 GeV shift in the Higgs mass prediction.

The sensitivity of the Higgs mass prediction to δ is also shown in Figure 3. The dashed lines show the predictions for $\delta = \pm 0.1$, with \tilde{m} fixed to 10^{14} GeV. In the small y region there is an important suppression of the correction from δ : for δ of 10% the Higgs mass changes by only about 1%. This is due to the convergence property of the RG trajectories of λ , discussed in [12]. Remarkably, in the large

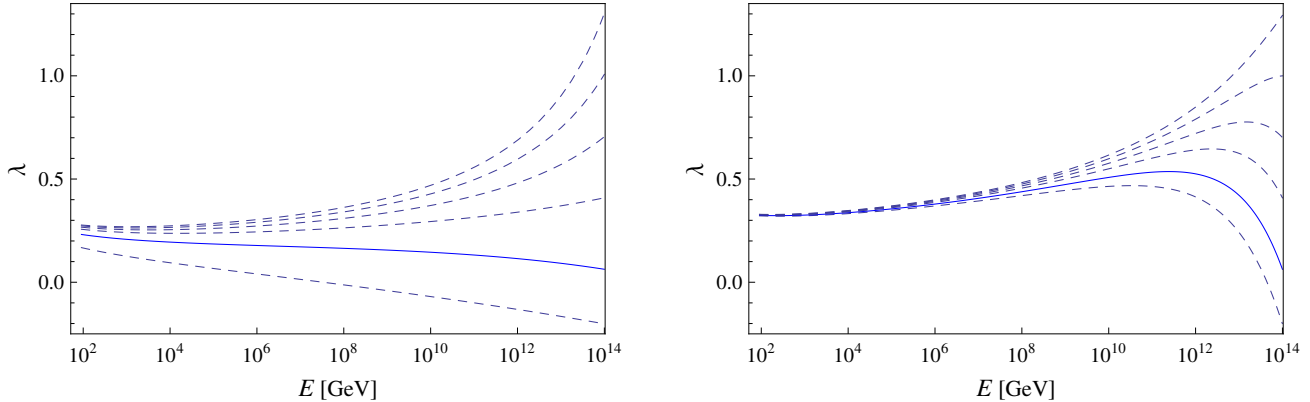


Figure 4: Evolution of the Higgs quartic coupling λ for $y(M_Z) = 0.7$ (left panel) and 0.9 (right panel). The curves represent $\lambda(\tilde{m}) = 0.06$ (the supersymmetric value; solid), $-0.2, 0.4, 0.7, 1.0, 1.3$ (dashed), where $\tilde{m} = 10^{14}$ GeV. A strong infrared convergence behavior eliminates the sensitivity of the Higgs boson mass to $\lambda(\tilde{m})$ for $y(M_Z) = 0.9$.

y region, this convergence behavior is much stronger so that, by $y = 0.8$, δ becomes irrelevant and one begins to lose sensitivity to the value of the supersymmetric boundary condition itself.

To understand this behavior, in Figure 4 we plot several trajectories for λ , with $y(M_Z) = 0.7$ and 0.9 for a fairly wide range of $\lambda(\tilde{m})$. Since y grows in the ultraviolet it is significantly above unity near \tilde{m} , and the y^4 term in the RG equation for λ causes the quartic to rise rapidly on scaling below \tilde{m} . Thus λ quickly loses its initial value and is largely determined by y . Indeed, we see that in much of the large y region the Higgs mass is linear in y , corresponding to $\lambda \propto y^2$ at the weak scale, reflecting the structure of the leading terms in the RG equation for λ . Therefore, the Higgs mass prediction at large y is, in fact, more general than the supersymmetric boundary condition. It arises in any theory where the SM is augmented by a weak scale vector-like lepton doublet and Majorana singlet, providing the initial value of the quartic coupling is not too large and one of the two new gauge invariant Yukawa couplings is somewhat small.

In our model, because of the extreme insensitivity to $\lambda(\tilde{m})$ discussed above, we need not compute δ at large y . This is fortunate, because in this region there is a large contribution to δ proportional to y^4 , and y is greater than unity at the high scale. For the small y region this contribution is suppressed, and the other contributions to δ are the same as arise when the low energy theory is the SM, and have been computed and discussed in detail in [12]. In particular, there is a contribution from top squark loops that depends on the dimensionless trilinear coupling parameter $A_t/m_{\tilde{t}}$, giving $\delta_{\tilde{t}} \sim 0.01 - 0.03$ for $A_t/m_{\tilde{t}} = 1 - 3$. In addition, with seesaw neutrino masses there could be a contribution, δ_ν , if the neutrino Yukawa coupling is of order unity. This is significant only if a right-handed neutrino mass, M_R , satisfies $M_R \gtrsim 10^{14}$ GeV and $M_R < \tilde{m}$, in which case the Higgs mass prediction could be affected at the 1 GeV level. Finally, it may be that threshold corrections from grand unification are present, but again we stress that a 10% correction to δ only affects the Higgs mass at the 1% level.

<i>s</i> -wave	channel
$\chi_1^0 \chi_1^0 \rightarrow ZZ$	<i>t</i> -channel χ_i^0 ($i = 1, 2, 3$) exchange
$\chi_1^0 \chi_1^0 \rightarrow W^+ W^-$	<i>t</i> -channel chargino exchange
$\chi_1^0 \chi_1^0 \rightarrow ff$	<i>s</i> -channel <i>Z</i> exchange and <i>s</i> -channel Higgs exchange
$\chi_1^0 \chi_1^0 \rightarrow hZ$	<i>t</i> -channel χ_i^0 ($i = 1, 2, 3$) exchange

Table 2: Annihilation channels for *s* wave.

<i>p</i> -wave	channel
$\chi_1^0 \chi_1^0 \rightarrow ZZ$	<i>s</i> -channel Higgs exchange
$\chi_1^0 \chi_1^0 \rightarrow W^+ W^-$	<i>s</i> -channel Higgs exchange and <i>s</i> -channel <i>Z</i> exchange
$\chi_1^0 \chi_1^0 \rightarrow hh$	<i>s</i> -channel Higgs exchange and <i>t</i> -channel χ_i^0 ($i = 1, 2, 3$) exchange
$\chi_1^0 \chi_1^0 \rightarrow hZ$	<i>s</i> -channel <i>Z</i> exchange

Table 3: Annihilation channels for *p* wave.

4 Dark Matter

In this section, we study constraints imposed on the parameter space by the requirement of dark matter. We assume the standard picture of inflation, followed by a radiation dominated era with high temperature. The dark matter particles are produced in the thermal plasma, and their abundance is determined by a standard thermal freezeout computation.

The singlino and the neutral Higgsinos mix to form neutralinos, and their mass matrix can be read off from the Lagrangian of Eq. (3). In the $(\tilde{s}, \tilde{h}_d^0, \tilde{h}_u^0)$ basis, the matrix is given by

$$M_{\chi^0} = \begin{pmatrix} m & yv & 0 \\ yv & 0 & -\mu \\ 0 & -\mu & 0 \end{pmatrix}. \quad (7)$$

The lightest mass eigenstate χ_1^0 is identified with dark matter. In addition to the three neutralinos, there is also one chargino state from \tilde{h}_u^+ and \tilde{h}_d^- , with a mass μ . Once the neutralino mass matrix is diagonalized, we can express the Lagrangian in the mass basis and compute all the relevant couplings. In the following subsections, we study constraints on the parameters y , m and μ from relic density and direct detection of dark matter.

4.1 Relic abundance

The thermally-averaged dark matter annihilation cross section times the velocity may be expanded as $\langle \sigma v \rangle = a + bv^2$ for small velocities. The first term is the *s*-wave contribution, while the second term the *p*-wave contribution. The channels contributing to the *s* and *p*-wave annihilations in our model are shown in Tables 2 and 3.

The cross sections for some of these channels depend on the Higgs boson mass, which depends on the Yukawa coupling y . To incorporate this dependence we fit the curve in Figure 2 to get a functional form for the $M_H(y)$. Since the allowed range in y is fairly small, a polynomial provides a very good fit.

Co-annihilation contributions become significant once the neutralino masses become comparable (when $\mu \sim m$), and we perform our calculation using micrOMEGAs [15] to incorporate this effect.

In Figure 5, we show the regions in μ - m planes in which the dark matter abundance is consistent with the observed value, $\Omega_{\text{DM}}h^2 = 0.1131 \pm 0.0034$ [16], for $y = 0.2, 0.4, 0.6,$ and 0.9 (in red). Contours for the dark matter mass are shown as dashed curves. In the plots, we also show “anthropic” windows, which correspond to the regions where the dark matter relic abundance is within a factor of 2 (medium blue) and 10 (light blue) from the central value of observations. The choice we made for the widths of the anthropic windows is arbitrary, but it illustrates some generic situation in environmental selection for dark matter in our model.

Suppose that the masses of the singlino and Higgsinos, m and μ , scan in the multiverse, with the distributions more or less flat in logarithms. In this case the distribution function is approximately flat in the μ - m planes of Figure 5, so that for a given y , the probability of finding m and μ in a certain region is proportional to the area of the anthropic window there. We then find from Figure 5 that for $y \lesssim 0.2$, we most likely find $\mu \sim \text{TeV}$ and $\tilde{m} \gtrsim \text{TeV}$, as the anthropic window has the largest area there. This is the region in which dark matter is mostly a pure Higgsino, of mass $\sim \text{TeV}$, with a small mixture with the singlino. (The plots are obtained using micrOMEGAs, which does not include the effect of Sommerfeld enhancement for annihilation. Inclusion of this effect will shift the values of μ larger in this region by a few % [17].) On the other hand, for $y \gtrsim 0.6$, we find that regions with small dark matter masses become larger, so that the probability of finding ourselves in one of these regions is significant. In these regions, dark matter is a mixture of the singlino and Higgsinos, and has a mass below $\sim 300 \text{ GeV}$. At what value of y the transition of the two regimes occurs? This depends on the width of the anthropic window. For a relatively small window, having a light dark matter regime with a significant probability requires rather large y , e.g. $\gtrsim 0.6$, as indicated by the medium blue regions in the figure. For a large window, however, there is a significant probability of obtaining light dark matter already for $y \sim 0.4$, as can be seen by looking at the light blue regions in the figure.

In the case that only the symmetry breaking parameter ϵ scans in the multiverse, the ratio between m and μ is fixed. In this case, scanning occurs along a line with a fixed slope in the μ - m plane. Assuming that the distribution of ϵ is approximately flat in logarithm, the situation is almost the same as above for $m/\mu \gtrsim 1$. For $m/\mu \lesssim 1$, however, the mostly Higgsino case cannot be realized, and light dark matter regions result.

Phenomenology of our model depends crucially on the parameter region we are in. As we saw above, this depends on the assumption on the multiverse distribution of parameters, including which parameters do or do not scan, as well as the width of the anthropic window for dark matter abundance. The relative preference between the light and Higgsino dark matter regions is also changed if the distribution of m or μ deviates from logarithms. We therefore consider both these cases when we analyze phenomenology of the model in later sections.

4.2 Direct detection

In addition to the bound from its abundance, dark matter is also subject to experimental constraints from direct detection searches. In Figure 5, we show contours of the spin-independent cross section between dark matter and a nucleon. We find that the current upper bound from existing experiments permits the entire parameter space shown. This can be understood as follows. Since the dark matter particle is in general a mixture of the neutral components of the Higgsinos and the singlino, it is a Majorana fermion,

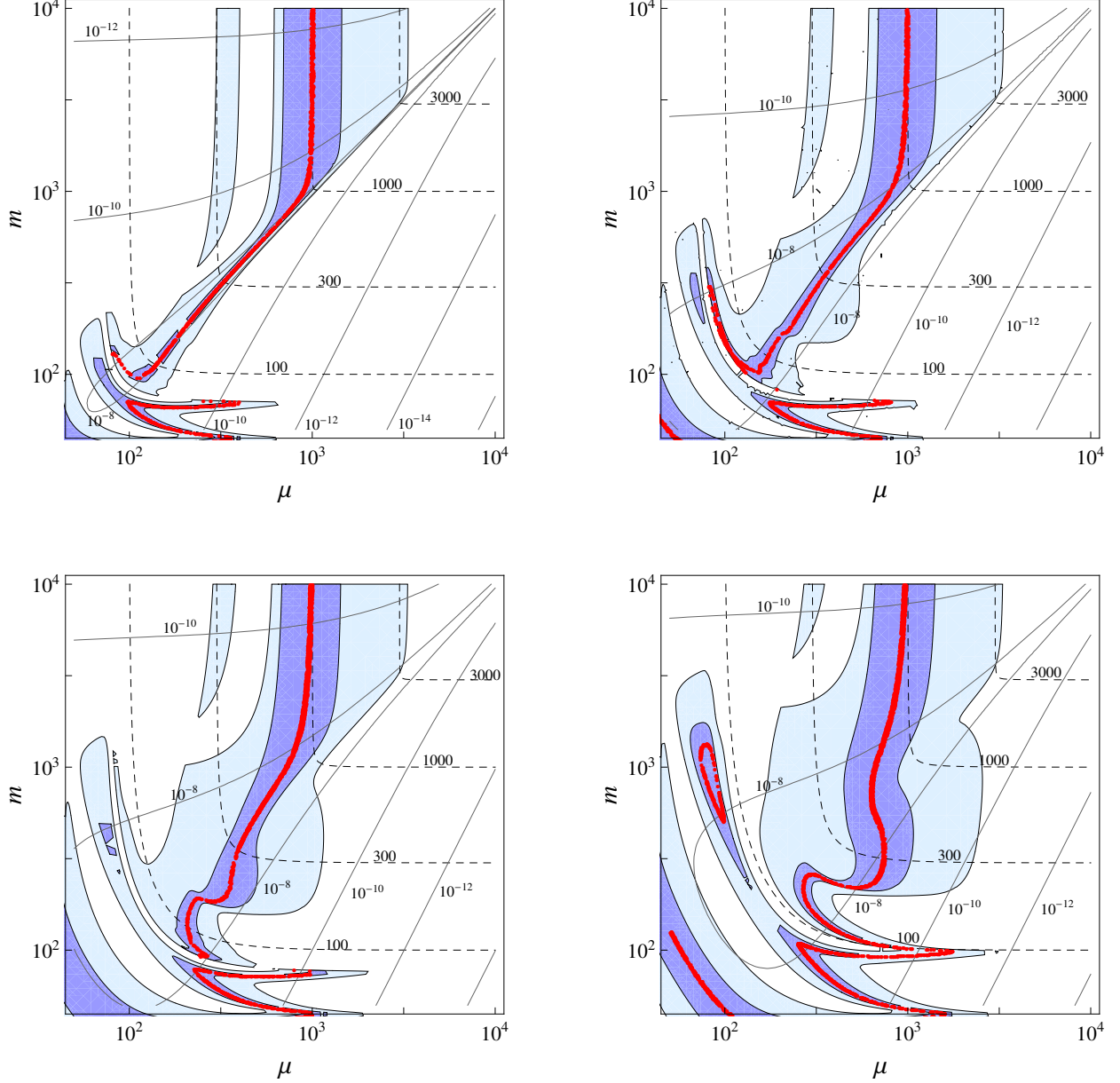


Figure 5: Regions reproducing the observed dark matter abundance on the $\log \mu$ - $\log m$ planes (red) for $y = 0.2$ (upper left), 0.4 (upper right), 0.6 (lower left), and 0.9 (lower right). The “anthropic” windows are also shown in each plot, representing the regions in which the dark matter abundance is within a factor of 2 (medium blue) and 10 (light blue) from the central value of observations. The relic abundance is calculated using micrOMEGAs, which does not include the Sommerfeld effect for annihilation. Inclusion of this effect will shift the values of μ for the vertical, mostly-Higgsino corridors larger by a few %. Contours for the dark matter mass (in GeV) are also shown as dashed curves, while those for the spin-independent cross section between dark matter and a nucleon (in pb) are shown as solid curves.

so that its coupling to the Z boson is suppressed. The dominant contribution to the cross section then comes from Higgs exchange. In most of the parameter region, this contribution is suppressed by the mixing between the Higgsino and singlino components, and hence small. For $|\mu - m| \sim 100$ GeV the mixing can be large, but the cross section is still small enough to evade the current bound.

In the future, experiments such as XENON, LUX and LZ20 are expected to lower the upper bound on the cross section and will probe a significant portion of the parameter space of the model. This will be discussed in more detail in section 5.3.

5 Experimental Signals

In this section, we discuss potential experimental signals which could probe the model in the near future. We mainly consider experiments which are either already taking data or will start taking data “soon.” These include measurements at the Tevatron and the LHC, dark matter direct detection experiments like XENON, LUX, LZ20, etc., and indirect detection experiments like HESS, VERITAS, MAGIC, FERMI/GLAST, etc. We now look at each of these in some detail.

5.1 Higgs mass measurements at the Tevatron and the LHC

From Figure 2, we see that the Higgs boson mass ranges from $\simeq 141$ GeV to ≈ 210 GeV for the entire perturbatively allowed range of y . For this range of the Higgs boson mass, the production cross section at the Tevatron—coming from gluon fusion (gg), associated production (Wh, Zh), and vector boson fusion (VBF)—is sizable, ranging from ~ 830 fb to ~ 195 fb [18]. By combining results from all available CDF and D0 channels on SM-like Higgs searches with luminosities $2.0 - 4.8\text{fb}^{-1}$ and $2.1 - 5.4\text{fb}^{-1}$, respectively, the Tevatron has already excluded an SM-like Higgs boson at 95% C.L. in the mass range $163\text{ GeV} < M_H < 166\text{ GeV}$ [19]. With more data and future improvements on the analysis, the Tevatron will be able to probe a wider range for the Higgs mass around this region.

A real discovery of the Higgs boson, however, will have to wait the LHC. In fact, the LHC can cover the entire Higgs mass range of the model relatively easily. This can be seen, for example, from Figure 13 of Ref. [20] where it is shown that the $h \rightarrow WW$ and $h \rightarrow ZZ$ channels can be used to make a 5σ discovery of a SM-like Higgs boson in the above mass range with about 10fb^{-1} of data. The best channel for the determination of the Higgs mass in this mass range is $h \rightarrow ZZ \rightarrow 4l$ with one of the Z s being real or virtual depending on the Higgs mass. It has been claimed in [21, 22] that the statistical precision on the Higgs mass at CMS and ATLAS with 30fb^{-1} data at the LHC is $\sim 0.1\%$. The systematic uncertainty on the absolute energy scale for leptons is expected to be around the same or less; for example, the goal of ATLAS is to determine the lepton energy scale to 0.02%. Hence, the Higgs mass can be determined very precisely in the mass range relevant here. This is, in fact, crucial in making an accurate determination of y from the Higgs boson mass, which can then be tested by other measurements.

5.2 LHC signals

We now discuss prospects for probing our model at the LHC. The possible production modes for the new TeV states are $q\bar{q} \rightarrow \chi_1^+ \chi_1^-$, $\chi_i^0 \chi_j^0$; $q\bar{q}' \rightarrow \chi_1^+ \chi_i^0$; and $gg \rightarrow \chi_i^0 \chi_j^0$ through an intermediate on-shell Higgs boson produced via top-loop. The possible decay modes are $\chi_3^0 \rightarrow \chi_{1,2}^0 Z$, $\chi_1^\pm W^\mp$; $\chi_1^\pm \rightarrow \chi_1^0 W^\pm$; and $\chi_2^0 \rightarrow \chi_1^0 Z$. The signatures are, therefore, based on “short cascades” in contrast to the “long cascades” in traditional supersymmetry. The best signals arise when the W and Z bosons decay leptonically giving rise

to various numbers of leptons and missing energy. The hadronic channels suffer from larger backgrounds, but a larger branching ratio of the weak bosons to hadrons suggests that a detailed investigation may be necessary. Here we focus on the leptonic channels. The signatures are similar to those studied in [23], except that the Higgs mass was quite heavy in the model considered there.

From the analysis in Ref. [23], one finds that even if one restricts to leptonic channels, those with a) 1 lepton + \cancel{E}_T and b) 2 leptons + \cancel{E}_T do not provide good prospects. This is because of the huge SM backgrounds. For channel a), the dominant backgrounds are Drell-Yan $W^{(*)}$ production, WZ production and $t\bar{t}$ production, and they swamp the signal even for parameter regions with large cross sections. For channel b), which arises from the production of $\chi_i^0\chi_1^0$ and $\chi_1^+\chi_1^-$, the dominant backgrounds are from WW , ZZ , WZ and $t\bar{t}$ production. By looking at the H_T ($\equiv \sum_{\text{visible}} |p_T|$) distribution after applying appropriate cuts, one finds that the background and signal are very similar in shape. For large cross sections of ~ 200 fb, it may be possible to get a good signal significance after optimizing the cuts for about 100 fb^{-1} of data. In Ref. [23], however, the large enhancement in the production cross section for $\chi_i^0\chi_1^0$ arose from the Higgs production mode, with $h \rightarrow \chi_i^0\chi_1^0$ for a heavy enough Higgs boson. This mode is not available in our model, so channel b) does not provide good prospects either.

Channel c) with 3 leptons + \cancel{E}_T provides better prospects. Search strategy in this channel is similar to that for direct chargino-neutralino production in standard supersymmetry, with some differences. Analyses for the mSUGRA model for the trilepton channel have been performed in detail in [24] for ATLAS and in [21] for CMS. A more general MSSM model has been studied in [25] which is better suited for comparing to our model. In the limit where the squarks and sleptons are heavy, $\chi_1^+\chi_{2,3}^0$ production proceeds through the same diagrams both for the MSSM and our model, with the dominant one being Drell-Yan production via s -channel W exchange. The dominant SM backgrounds are from $t\bar{t}$ production with both tops decaying leptonically and the third lepton coming from a semileptonic decay of the b or a jet fake, and WZ production with both W and Z decaying leptonically. In the MSSM, there is also a large supersymmetry background from gluino pair production and gluino squark production. If gluino and squarks are much heavier than the charginos and neutralinos, these supersymmetry backgrounds can be minimized. Also, in these analyses the parameter region $m_{\chi_2^0} - m_{\chi_1^0} < M_Z$, in which an opposite sign, same flavor (OSSF) pair of leptons arises from an off-shell Z , is mostly studied as this is quite helpful in reducing the WZ background in the dilepton mass distribution where the Z is on-shell and decays to two OSSF leptons. Apart from the Z -mass cut, the other important cuts applied in [24, 21, 25] are: 1) At least three isolated leptons, 2) One pair of OSSF leptons, and 3) No jets with $p_T > 30$ GeV (optional). Figure 4.17 in [25] shows the 5σ sensitivities with 30 fb^{-1} and 100 fb^{-1} of data at the LHC in the μ - M_2 plane (with $M_2 = 2M_1$), where μ is the Higgsino mass and M_2, M_1 are the wino and bino mass parameters in the MSSM.

What does this imply for our model? Since the production and decay modes for the channels considered here are identical between our model and the MSSM, one expects that the production cross section times branching ratio ($\sigma \times \text{Br}$) is also roughly similar. This implies that for channel c), the regions with cross sections $\sim 10 - 50$ fb could be probed in our model. In Figure 6, the regions in the μ - m plane which are consistent with i) the LEP constraint on the chargino mass ($m_{\chi_1^+} > 103$ GeV [14]) and ii) the Z -mass cut ($m_{\chi_2^0} - m_{\chi_1^0} < M_Z$) are shown in white (unshaded), for four different values of y . The regions iii) leading to the WMAP allowed relic abundance [16] are also depicted with red bands. The unshaded regions within the range of the plots lead to production cross sections of roughly $O(10 - 50 \text{ fb})$, and hence should be probed with around 100 fb^{-1} of data, using the method similar to that described above. We then find that for small $y \lesssim 0.4$, the region $103 \text{ GeV} < \mu \lesssim (130 - 200) \text{ GeV}$ and $50 \text{ GeV} \lesssim m \lesssim (140 - 150) \text{ GeV}$,

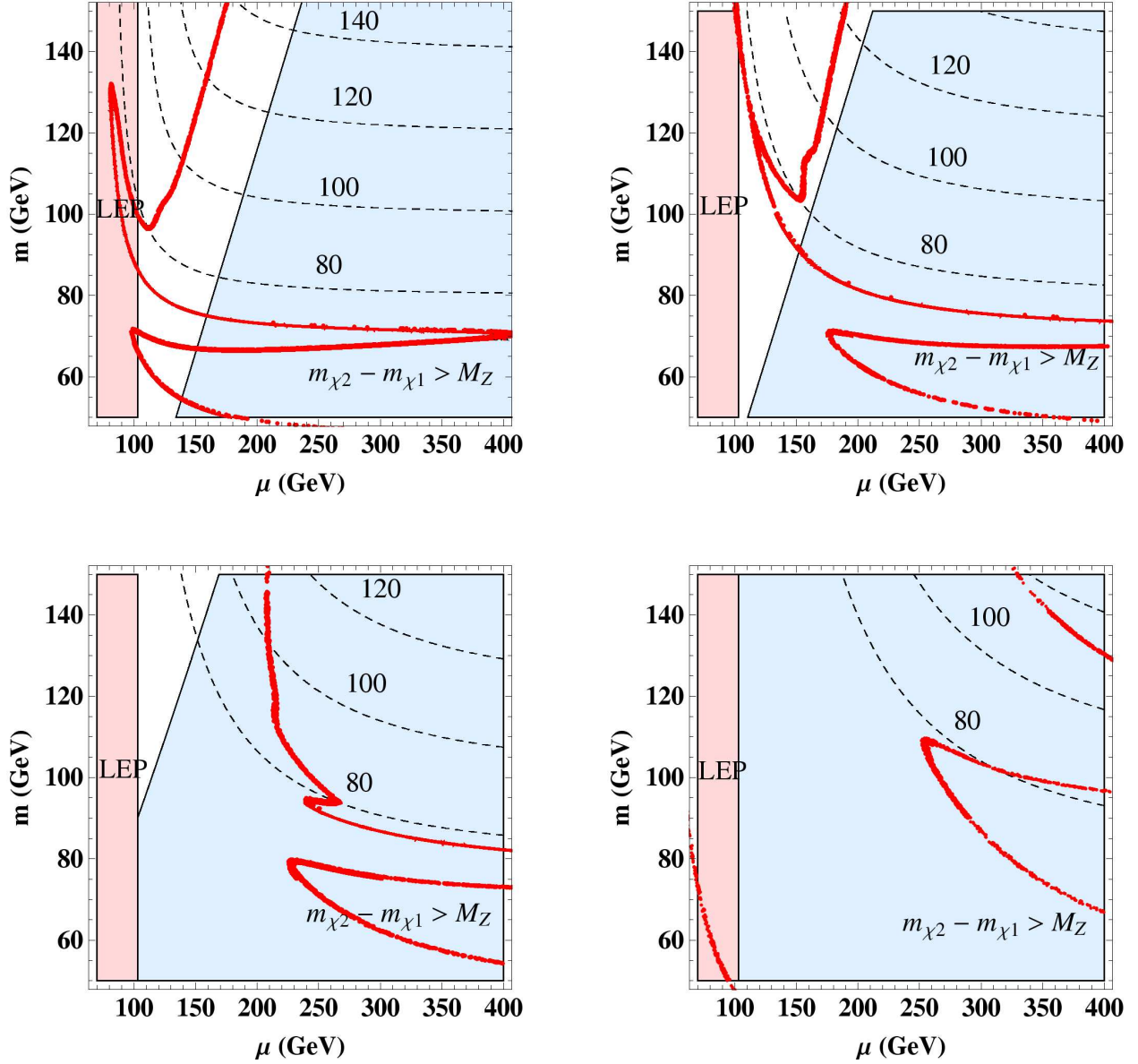


Figure 6: Regions consistent with the LEP constraint on the chargino mass, $m_{\chi_1^+} > 103$ GeV, and the Z-mass cut, $m_{\chi_2^0} - m_{\chi_1^0} < M_Z$, on the μ - m planes (unshaded regions) for $y = 0.2$ (upper left), 0.4 (upper right), 0.6 (lower left), and 0.9 (lower right). The red bands correspond to the parameter regions consistent with the WMAP bound on the dark matter relic abundance. Contours for the dark matter mass (in GeV) are also drawn as dashed curves.

which corresponds to $m_{\chi_1^0} \lesssim (120 - 140)$ GeV, can be probed at the LHC with 100 fb^{-1} of data. For larger values of y , however, the region consistent with i) and ii) shrinks and the WMAP constraint iii) is not satisfied. Thus, it is very hard to probe these regions at the LHC with analysis similar to [24, 21, 25], even with large amount of data.

It is also important to know if precise measurements of the model parameters can be made for the parameter regions that can be probed at the LHC. An observation of the dilepton invariant mass edge from OSSF leptons arising from an off-shell Z boson can, in principle, determine the mass difference $m_{\chi_{2,3}^0} - m_{\chi_1^0}$. Since the systematic uncertainty on the lepton energy scale is quite small ($\lesssim 0.1\%$), the uncertainty is dominated by statistics. It turns out that with a cross section of $10 - 50 \text{ fb}$ the number of signal events after imposing cuts with 100 fb^{-1} of data is only $O(100)$, and is about $2.5 - 3$ times smaller than the SM background [25]. Thus, the statistical precision of the measurement is limited by the bin size, which has to be large to contain enough events such that they are sufficiently above the fluctuation of the background. A rough estimate from the analysis in [25] gives the precision to be around 10% . Of course, the precision can be improved with more data, but given that the statistical precision with 100 fb^{-1} of data is about 10% , the precision can only be increased by a factor of few. A more detailed analysis is needed to obtain a better estimate of the precision, however.

5.3 Direct detection of dark matter

Since the reach of the LHC is only limited to small dark matter masses ($m_{\chi_1^0} \lesssim 140 \text{ GeV}$) as seen in the previous subsection, it is important to look at prospects for probing the model with direct dark matter detection experiments. As we saw in section 4.2, the entire parameter space of our model is allowed with existing bounds. This is because the Z -exchange contribution is highly suppressed, while the Higgs exchange contribution is still small. The one-loop contribution to the cross section generated by gauge interactions, which could be important for the mostly Higgsino-like case [26], turns out to be insignificant for model parameters satisfying the WMAP relic abundance constraint.

In Figure 7, we scan over values of μ and m allowed by the WMAP result on the relic abundance for four different values of y , and plot the corresponding spin-independent cross section on a proton σ_{SI}^p , calculated using micrOMEGAs. The scan is performed over the region where $m < 10 \text{ TeV}$, motivated by our theoretical construction in section 2. It is quite promising that the *entire* region of this parameter space will be probed by future generations of direct detection experiments. In particular, dark matter masses in the range $100 \text{ GeV} \lesssim m_{\chi_1^0} \lesssim 700 \text{ GeV}$ can be probed relatively soon for the entire range of y , by XENON and LUX. To probe heavier dark matter, more advanced detectors are required. For example, to probe the largest dark matter masses around a TeV, the highly advanced LZ20T detector, with a sensitivity about three orders of magnitude better than that of LUX 300kg, will be needed.

In addition to the detection of dark matter, it is important to address how precisely the mass and cross section can be determined from these experiments. This has been studied in a number of papers, the most relevant ones being [28, 29, 30]. Here we follow the results of [28]. It was shown there that with data from only one experiment, the dark matter mass combined with its spin-independent cross section can be determined by a maximum likelihood analysis, comparing a theoretically predicted spectrum to measured recoil energies. For small dark matter masses ($m_{\chi_1^0} < m_{\text{nucleus}}$), the shape of the recoil spectrum is sensitive to the mass, enabling us to determine the mass (as well as the cross section) with modest accuracy. For example, for a dark matter mass of 50 GeV and spin-independent cross section of 10^{-7} pb , the statistical uncertainty for the mass turns out to be around 10% with a reasonably large exposure of

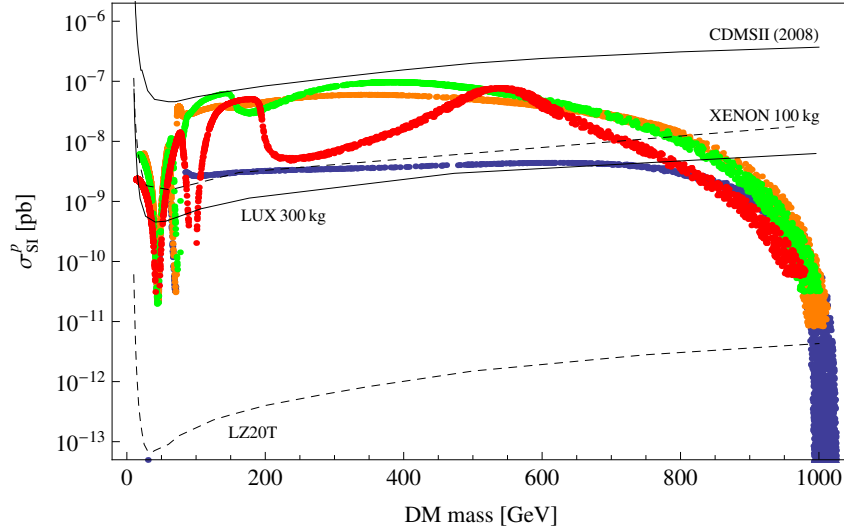


Figure 7: Predictions for the spin-independent cross section of dark matter on a proton, obtained by scanning μ and m for four different values of y : $y = 0.1$ (blue), 0.4 (orange), 0.6 (green) and 0.9 (red). The densities of the dots are the results of the scan, and do not have particular significance. Also shown are existing bounds from CDMSII and projected 90% C.L. upper limits from XENON 100kg, LUX 300kg, and LZ20T; these curves are obtained using Ref. [27].

3×10^5 kg · days. The statistical uncertainty worsens to about 20% if the mass is raised to 100 GeV with the same cross section and exposure. For dark matter masses above 100 GeV, the uncertainty increases drastically because the recoil spectrum is insensitive to the mass. In addition, with data from only one experiment, the mass determination described above depends on the assumptions about the velocity profile and also the local dark matter density. For example, for a dark matter mass of 100 GeV, a 10% error in the velocity distribution will cause a 20% systematic error in the mass determination, with a $\sim 10\%$ error in the spin-independent cross section.

With data from two or more experiments, however, it is possible to obtain the dark matter mass without any assumption about the velocity profiles or the local density. This is because the normalized (one-dimensional) velocity distribution $f_1(v)$ can be solved directly from the expression for the direct detection rate, and is independent of the spin-independent cross section and the local halo density [29]. However, it does depend on the masses of the nucleus and the dark matter. Thus, by requiring that the values of a given moment of the distribution $f_1(v)$ agree for two experiments with nuclei X and Y , it is possible to measure the dark matter mass $m_{\chi_1^0}$ in a model-independent way. For $m_{\chi_1^0} \lesssim 100$ GeV, it is possible to measure the dark matter mass to $\lesssim 20\%$ with $O(500)$ events (before cuts) for two target nuclei ^{28}Si and ^{76}Ge . For masses above 100 GeV, however, the algorithmic procedure for determining the masses does not provide reliable estimates. Finally, by making an assumption about the local dark matter density, it is also possible to measure the spin-independent cross section with a statistical uncertainty of $\sim 15\%$ with $O(50)$ events for $m_{\chi_1^0} \lesssim 100$ GeV, without any assumption about the dark matter mass or its velocity profile. Again, the uncertainty in the measurement of the cross section increases drastically for $m_{\chi_1^0} \gtrsim 100$ GeV [28].

5.4 Indirect detection of dark matter

In addition to direct detection, dark matter can also be detected through products of its annihilation in the galactic halo, which gives rise to many kinds of cosmic rays such as photons, neutrinos, electrons, positrons, protons and antiprotons. Since the annihilation cross section of dark matter is determined by the measured relic abundance, and since there is no significant enhancement of the cross section from the epoch of freezeout to the present, the indirect detection signals from electrons and positrons, protons and antiprotons, and diffuse photons and neutrinos are not very promising as they are typically overwhelmed by the background.

However, the processes $\chi_1^0\chi_1^0 \rightarrow \gamma\gamma$ and $\chi_1^0\chi_1^0 \rightarrow \gamma Z$ are induced at loop level, leading to monochromatic γ -ray with energies $E_\gamma = m_{\chi_1^0}$ and $E_\gamma = m_{\chi_1^0} - M_Z^2/4m_{\chi_1^0}$, respectively. This gives rise to sharp lines in the photon spectrum which have much better prospects for detection. Adapting the detailed computation of σv given in [31] to our model, we find that $\sigma v(\chi_1^0\chi_1^0 \rightarrow \gamma\gamma)$ reaches a relatively large constant value ($\approx 10^{-28}$ cm³/s) for Higgsino-like dark matter with mass \gtrsim TeV. A more precise treatment of this case should include non-perturbative effects involving both dark matter and its $SU(2)_L$ partner(s) (the Sommerfeld enhancement) [32]. However, since including these effects changes $\sigma v(\chi_1^0\chi_1^0 \rightarrow \gamma\gamma)$ by at most $O(30\%)$ for dark matter masses satisfying the relic abundance constraint, we use the perturbative computation of [31] in our analysis, for simplicity.

The detectors best suited for detecting γ lines are atmospheric Cherenkov telescope (ACT) detectors like VERITAS, HESS, MAGIC, etc. and satellite-borne γ -ray detectors like FERMI/GLAST. Although the ACT detectors have a small angular acceptance and a higher energy threshold, they have a much larger area than satellite-based telescopes like FERMI/GLAST. So, they are ideal when a large monochromatic photon flux is emitted from a small region of the sky such as from the Galactic Center, whose coordinates are known with sufficient accuracy. This also means that they are strongly sensitive to the dark matter profile and provide better prospects for steeper profiles like NFW or Moore. The sensitivity of ACT detectors is determined by a relatively large background of misidentified gamma-like hadronic showers and cosmic-ray electrons, with the contribution from the diffuse γ -ray background being mostly subdominant. MAGIC currently provides the best sensitivity for γ -rays with energies larger than 300 GeV; the sensitivities of HESS and VERITAS are very similar. Advanced detectors like AGIS and CTA, which will come online in future, have the potential to reach much better sensitivities than the detectors above [33], although their physical location will determine their ability to observe the Galactic Center. The 5σ point-source sensitivities of MAGIC, VERITAS and HESS for continuous γ -rays are given in [31, 34], which we adopt in our analysis. (The sensitivities for the γ -lines are in fact expected to be somewhat better.) There are, however, two important sources of uncertainties in these detectors. First, these detectors have a 10 – 20% energy resolution which smears the line shape and decreases the sensitivity. Second, there is an overall systematic uncertainty in the energy scale, $\sim 30\%$ for MAGIC and $\sim 15\%$ for HESS, which provides the dominant uncertainty in the determination of the dark matter mass.

Unlike ACT detectors, satellite detectors have a much larger angular acceptance and a lower energy threshold. These detectors look at a large part of the galaxy; hence they are much less sensitive to the dark matter profile. Therefore, detectors like FERMI/GLAST provide the best sensitivity for less steep profiles. Since the background rejection from hadronic showers and cosmic electrons is much better for these detectors, their sensitivity is only limited by counting statistics and the diffuse γ -ray background. The 5σ sensitivity for a five-year operation of FERMI/GLAST is given in [35].

The Galactic Center is ideal for the detection of the gamma-ray monochromatic signal because of the

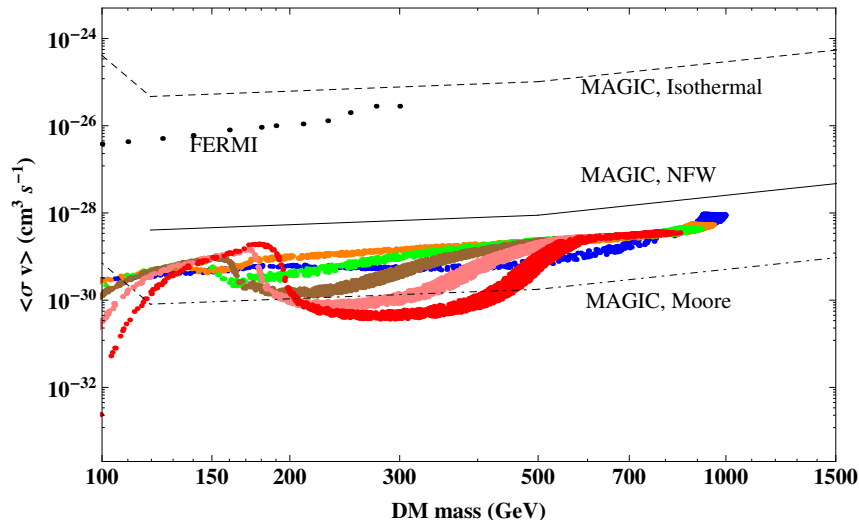


Figure 8: Predictions for $\sigma v(\chi_1^0 \chi_1^0 \rightarrow \gamma\gamma)$ by scanning μ and m for six different values of y ; the blue, orange, green, pink, brown, and red dots correspond to $y = 0.1, 0.4, 0.6, 0.7, 0.8,$ and $0.9,$ respectively. Also shown are sensitivities of the MAGIC ACT detector (with one-year exposure) arising from the flux of a $\Delta\Omega = 10^{-5}$ sr cone encompassing the Galactic Center, for three different dark matter profiles: Moore, NFW and Cored Isothermal. The black dots represent the sensitivity of the FERMI/GLAST experiment, with five-year exposure to the flux of an annulus centered around the Galactic Center, but excluding the region within 15° of the Galactic plane.

extremely large dark matter density there. However, the presence of astrophysical point sources in the Galactic Center could present a serious background to the signal. In fact, an intense point-like gamma-ray source (J1745-290) has been observed by HESS [36]. One possible origin of this source is believed to be the stochastic acceleration of electrons interacting with the turbulent magnetic field of Sgr A*, the supermassive black hole at the center of our galaxy. In the following analysis, for simplicity we compute sensitivities for $\sigma v(\chi_1^0 \chi_1^0 \rightarrow \gamma\gamma)$ (for different profiles) assuming that this important background can be subtracted efficiently. A better (but more complicated) strategy may be to consider a larger angular region with a size depending on the dark matter profile as well as the morphology of background and signal emissions, and then subtract all detected astrophysical sources within this region [37].

In Figure 8, we show the results for $\sigma v(\chi_1^0 \chi_1^0 \rightarrow \gamma\gamma)$ by performing a scan over μ and m (allowed by the WMAP result for the relic abundance) for six different values of y , similar to what was done for direct detection. The sensitivities of ACT detector—MAGIC with one-year exposure to the Galactic Center point source—for three qualitatively different dark matter profiles, as well as the sensitivity of FERMI/GLAST with five-year exposure to an annulus around the Galactic Center, are also shown. It can be seen that existing ACT detectors like MAGIC, HESS or VERITAS provide better detection prospects than FERMI/GLAST for reasonably steep profiles. Still, they can only probe the model for very steep halo profiles like the Moore profile. Regarding these profiles, it is interesting to note that the presence of baryons is *not* taken into account in the various simulations leading to the above profiles. In principle, this could significantly affect the picture near the galactic center because of the interactions of the supermassive black hole with the surrounding dark matter distribution. Although a full understanding of

these effects is unavailable at present, in the “adiabatic compression” scenario which takes into account some of these interaction effects [38], the dark matter density near the galactic center is significantly increased relative to the NFW profile leading to a signal which is about three orders of magnitude larger than that for the NFW profile [39]! In this case, the entire parameter space of the model can be easily probed with the above ACT detectors.

The sensitivities quoted above may be improved if the energy resolution is improved or if the background from misidentified photons is further suppressed. Also the 2γ and γZ lines cannot be resolved for dark matter masses $\gtrsim 500$ GeV, in which case adding the γZ contribution will increase the effective cross section by a little more than a factor of two, making the detection prospects better. Also, as mentioned earlier, future detectors like AGIS and CTA are expected to have much better sensitivities and can probe a much larger parameter space of the model even for widely accepted profiles such as NFW. Moreover, with a better understanding of the systematics, the dark matter mass can be measured to better than $\sim 15\%$.

6 SM + Wino as an Effective Theory below the Unified Scale

Environmental selection of dark matter may prefer a light wino, so that the effective theory below \tilde{m} is SM + \tilde{w} . In this case the theory at \tilde{m} need not have a singlet—the MSSM states are enough to lead to consistent phenomenology at low energies. For \tilde{m} not far from the unified scale, $\sim 10^{14}$ GeV, this setup leads to the following prediction for the Higgs boson mass [12]. The Higgs mass M_H is in the range $127 \text{ GeV} \lesssim M_H \lesssim 142 \text{ GeV}$, where we have included two-loop RG effects from the wino. In particular, for large $\tan\beta$

$$M_H \simeq 141.5 \text{ GeV} - 0.4 \text{ GeV} \left(\frac{10}{\tan\beta} \right)^2 + 1.8 \text{ GeV} \left(\frac{m_t - 173.1 \text{ GeV}}{1.3 \text{ GeV}} \right) - 1.0 \text{ GeV} \left(\frac{\alpha_s(M_Z) - 0.1176}{0.002} \right). \quad (8)$$

This prediction is subject to errors coming, e.g., from (a few orders of magnitude) uncertainty for the value of \tilde{m} , supersymmetric threshold corrections at \tilde{m} , and higher order corrections. These errors, however, give only a few hundred MeV corrections to M_H [12], so that the prediction is very precise.

The wino $\tilde{w} = (\chi^\pm, \chi^0)$ is an $SU(2)_L$ -triplet Weyl fermion, and has couplings to the standard model particles only via $SU(2)_L$ gauge bosons. The couplings are completely determined by gauge symmetry and therefore the only parameter in the model is the wino mass M_2 . The charged and the neutral winos are degenerate at tree level. After electroweak symmetry breaking, radiative corrections generate a mass splitting [40]

$$\delta m \equiv m_{\chi^\pm} - m_{\chi^0} = \frac{\alpha M_W}{2(1 + c_w)} \left(1 - \frac{3}{8c_w} \frac{M_W^2}{M_2^2} \right), \quad (9)$$

which is roughly 165 MeV for $M_2 \gg M_W$.

Since the only parameter in the model is the wino mass M_2 , assuming dark matter is thermal, M_2 can be determined by the observed dark matter relic density. Taking the range of the relic density consistent with the observation at 2σ , i.e. $0.106 < \Omega_{\text{DM}} h^2 < 0.120$, the wino mass is found, using micrOMEGAs, to be $2.24 \text{ TeV} < M_2 < 2.38 \text{ TeV}$. As M_2 is much larger than the weak boson mass M_W and the charged-neutral winos are nearly degenerate, however, the non-perturbative Sommerfeld effect can affect the relic density by as much as 30%. The effect can be estimated using the numerical result given in [17], where wino-like dark matter was studied. The wino mass consistent with the relic density turns out to

be

$$2.7 \text{ TeV} \lesssim M_2 \lesssim 3.0 \text{ TeV}. \quad (10)$$

This narrow window for M_2 , as well as the Higgs mass prediction of Eq. (8), are the main predictions of this theory. To test the theory experimentally, therefore, it is important to measure M_2 with certain precision.

With a large mass of Eq. (10), discovery of wino dark matter at the LHC is not possible. Dark matter direct detection is also hard as the only coupling of dark matter is to the chargino and W gauge boson. This coupling only allows either tree-level inelastic scattering or one-loop suppressed elastic scattering with nuclei. Due to the $O(100)$ MeV mass splitting, observation through inelastic scattering is not possible. The dark matter-nucleon elastic scattering cross section at one loop is given in Ref. [41] as about 2×10^{-9} pb. It is beyond the reach of XENON 100kg or LUX 300kg, but can be reached by SuperCDMS phase C and LZ20T. Detection of this 3 TeV wino is possible at future detectors but the dark matter mass can not be determined to better than 50%. The best measurement of the dark matter mass probably comes from indirect detection, especially that of monochromatic gamma lines.

The indirect detection of wino dark matter is possible due to a large Sommerfeld enhancement associated with the highly-degenerate and large wino masses. The most promising channel is the monochromatic gamma lines, which we will focus on. The cross section for $\chi^0 \chi^0 \rightarrow \gamma\gamma$ is calculated in Ref. [32]. For the M_2 mass range given above, the effective cross section is

$$\sigma_{\chi^0 \chi^0 \rightarrow \gamma\gamma} v \sim (2 - 0.6) \times 10^{-25} \text{ cm}^3/\text{s}. \quad (11)$$

Compared with the cross section without the Sommerfeld effect, this enhancement corresponds to a boost factor of 125 (40) for $M_2 = 2.7$ (3.0) TeV. As shown in Figure 8, this is within the reach of MAGIC even for the dark matter profile at the Galactic Center much shallower than NFW. The energy resolution is expected to be similar to lower energies, so that the mass of wino dark matter can be measured to 10 – 20% in the near future.

7 Discussion and Conclusions

A description of nature that contains unexplained fine-tunings is deeply unsatisfactory. There is no natural explanation for the observed size of the cosmological constant, and preliminary investigations of the weak scale have failed to uncover any sign of a natural explanation for the size of electroweak symmetry breaking. Yet both of these fine-tunings can be understood from environmental selection on a multiverse. The cosmological constant is close to a catastrophic boundary at which large scale structure fails to form [3], and the weak scale is close to a catastrophic boundary at which complex nuclei are unstable [4]. If the LHC fails to uncover a natural theory for the weak scale, then the evidence for the multiverse will be strengthened; if evidence is found that supports an elementary Higgs boson to very high energies, this strengthening will be highly significant.

An environmental weak scale is a profound change in our way of thinking about physics beyond the SM, and immediately leads to further questions. What is the scale of supersymmetry breaking, now that it has been logically disconnected from the weak scale? What is to be made of the success of precision gauge coupling unification that arose with weak scale supersymmetry? What is the nature of dark matter—in particular how is the WIMP hypothesis affected? More generally, what new physics is expected to be within reach of the LHC and future colliders?

	I	II	III
States at TeV scale	SM	(SM + \tilde{w})	(SM + \tilde{h}/\tilde{s})
Dark Matter	QCD axion	\tilde{w} E-WIMP	E-WIMP LSP
DM selection acts on	θ_{mis}	$m_{\tilde{w}}$	ϵ
New parameters	f_a, θ_{mis}	$m_{\tilde{w}}$	μ, m, y
Gauge coupling unif.	SM	\approx SM	\approx MSSM
Higgs mass	(128 – 141) GeV	(127 – 142) GeV	(141 – 210) GeV

Table 4: Comparison of the three realistic TeV-scale effective theories with high scale R breaking that result from environmental selection for dark matter in a supersymmetric theory containing the states of the MSSM and possibly additional gauge singlets. The supersymmetry breaking scale is taken to be very high, broadly of order the unification scale. Higgs mass values are for $m_t = 173.1$ GeV and $\alpha_s(M_Z) = 0.1176$.

It is striking that the dark matter and baryon densities in our universe differ by only a factor of five, while their microphysical origins are apparently unrelated. Furthermore, the formation of large scale structure is highly dependent on changes in the dark matter density relative to the baryon density, and it has been suggested that the dark matter density of our universe also arose from environmental selection [6]. This leads to the view that we espouse in this paper; that the physics at the TeV scale depends on the nature of the dark matter that is being selected. Before discussing the observable signals of the two models that we have studied in this paper, we give a comparison between some simple ways that this selection may occur in supersymmetric theories.

Suppose that at some scale \tilde{m} the SM is embedded in a supersymmetric theory. What are the TeV-scale effective theories that can result from environmental selection of both the weak scale and the dark matter abundance? In Table 4 (5) we show three theories that have a high (low) scale of R breaking in the observable sector. Indeed, if the dark matter particle is either an axion or a thermal relic composed of states of the MSSM, these are the *only* such theories that are allowed by experiment. (In the case of large R breaking we also allow gauge singlet states.)

In Theory I dark matter is composed of axions, with environmental selection acting on the axion misalignment angle θ_{mis} [43]. In Theories II – VI, dark matter is an Environmentally selected thermal relic, or E-WIMP, and is the lightest supersymmetric particle (LSP), with selection acting on different parameters to yield the dark matter abundance. In Theory II the selection acts on the mass of a particular superpartner, in particular the wino mass, so that there are cancellations between several large contributions leading to a TeV scale \tilde{w} , with all other superpartner masses of order \tilde{m} . In Theory III, the selection acts on the small symmetry breaking parameter ϵ of a non- R symmetry, allowing more than one mass parameter to be small. The Higgs mass predictions shown in Table 4 for Theories I, II and III follow from taking \tilde{m} very large, within one or two orders of magnitude of the scale of gauge coupling unification. The range in the Higgs mass arises from $\tan \beta$ in Theories I and II and from y in Theory III. If the theory at scale \tilde{m} has an approximate Peccei-Quinn symmetry, or if it is embedded into a higher dimensional theory with the Higgs doublets arising from a single supermultiplet, then the Higgs mass is predicted to lie at the upper end of the $\tan \beta$ range, leading to $M_H \simeq (141 - 142)$ GeV for Theories I and II (and Theory III with small y) [12].

Theories IV and V result from selection acting on an approximate R symmetry in the observable

	IV	V	VI
States at TeV scale	(SM + $\tilde{\lambda}$)	(SM + $\tilde{\lambda}/\hbar$)	E-MSSM
Dark Matter	\tilde{w} E-WIMP	E-WIMP LSP	E-WIMP LSP
DM selection acts on	ϵ_R	ϵ'_R	\tilde{m}
New parameters	$m_{\tilde{\lambda}}$	$m_{\tilde{\lambda}}, \mu, \tan \beta$	MSSM set
Gauge coupling unif.	SM	\approx MSSM	\approx MSSM
Higgs mass	(114 – 139) GeV	(114 – 154) GeV	\approx (114 – 130) GeV

Table 5: Comparison of the three TeV-scale effective theories with low scale R breaking that result from environmental selection for dark matter in a supersymmetric theory containing the states of the MSSM. In all three theories the gauginos, $\tilde{\lambda}$, are at the TeV scale. In Theories IV and V the scale of supersymmetry breaking ranges from unified scales to not far above the weak scale, when these theories merge with Theory VI. In addition to the parameters listed, Theory V (Split Supersymmetry) may involve two new physical phases. The lower bounds on the Higgs mass, 114 GeV, are due to experimental constraints [42].

sector, arising from a special form of the Kähler potential that suppresses the gaugino masses even in the presence of the large $U(1)_R$ breaking needed for a vanishing cosmological constant. Theory V has the μ parameter charged under this R symmetry so that all the fermionic superpartners are at the TeV scale, yielding Split Supersymmetry [7]. On the other hand, in Theory IV the μ parameter is not charged under the R symmetry, so that it is unsuppressed. This leaves only the gauginos at the TeV scale. Like Split Supersymmetry, this theory has a long-lived gluino, but the dark matter is necessarily pure \tilde{w} . Gauge coupling unification depends on \tilde{m} , and the precision is typically worse than in Split Supersymmetry. To avoid a cosmologically stable gluino, Theories IV and V require $\tilde{m} \lesssim 10^{10}$ GeV [44] or some additional light state to which the gluino can decay, such as an axino [45]. Hence the Higgs mass values quoted in Table 5 correspond to \tilde{m} varying from the TeV scale up to the unified scale. Finally, Theory VI results when the environmental selection acts on the supersymmetry breaking scale itself, so that all the superpartners are at the TeV scale.

Theories I, II and IV have gauge coupling unification with a precision comparable to that of the SM, while for Theories III, V and VI the precision is improved and is comparable to that of the MSSM. The unification scale is around 10^{14} GeV for Theories I, II and III, while it is around 10^{16} GeV for Theories IV, V and VI. For Theories II through VI, sufficient stability of the dark matter requires some symmetry, such as R parity.

Theory I has been studied in [12], which finds the theoretical uncertainties in the Higgs mass prediction to be remarkably small. In this paper we have studied the Higgs mass, hadron collider and astrophysical signals of Theories II and III. The phenomenology of Split Supersymmetry, Theory V, has been studied in detail over a wide range of values of \tilde{m} . The phenomenology of Theory VI is significantly different than that expected for the MSSM. In the MSSM, weak-scale supersymmetry is motivated to avoid a finely-tuned weak scale, and this gives constraints on the superpartner spectrum. In Theory VI the constraints on the spectrum are much less severe, since the only requirement is that the LSP is Environmentally selected dark matter; we call Theory VI the E-MSSM. In the E-MSSM a little supersymmetric hierarchy is *predicted* since \tilde{m} prefers to be as large as possible consistent with not over-producing dark matter. For example, the dark matter could be dominantly Higgsino with a mass near 1 TeV, or dominantly wino with a mass near 3 TeV, with other superpartners of order 10 TeV. Thus the dark matter signals of this

	I	II	III
States at TeV scale	SM	(SM + \tilde{w})	(SM + \tilde{h}/\tilde{s})
Dark Matter	QCD axion	\tilde{w}	\tilde{h}/\tilde{s}
New parameters	f_a, θ_{mis}	$m_{\tilde{w}} \simeq 3 \text{ TeV}$	μ, m, y
Higgs boson mass	(128 – 141) GeV	(127 – 142) GeV	(141 – 210) GeV
DM: large indirect γ signal	no	$\sigma v \sim 10^{-25} \text{ cm}^3 \text{ s}^{-1}$ $E_\gamma \simeq 3 \text{ TeV}$	no
DM: direct detection signal	no	$\sigma_{\text{SI}}^p \sim 2 \times 10^{-9} \text{ pb}$ $m_{\text{DM}} \simeq 3 \text{ TeV}$	$\sigma_{\text{SI}}^p \sim (10^{-9} - 10^{-7}) \text{ pb}$ for $100 \text{ GeV} \lesssim m_{\text{DM}} \lesssim 800 \text{ GeV}$
DM: small indirect γ signal	no	—	$\sigma v \sim (10^{-30} - 10^{-28}) \text{ cm}^3 \text{ s}^{-1}$ except $m_{\text{D}} \lesssim 100 \text{ GeV}$ and $m_{\text{DM}} \sim (200 - 500) \text{ GeV}$ for large y
LHC signals of new states	no	no	difficult; possible for low masses
signals at future lepton colliders	no	only with $\sqrt{s} \gtrsim 6 \text{ TeV}$	precise measurements of μ, m, y

Table 6: A comparison of the signals for Theories I, II and III. The supersymmetry breaking scale \tilde{m} is of order the unification scale $M_u \sim 10^{14} \text{ GeV}$. Beneath this scale the effective theory is the SM, together with the QCD axion, \tilde{w} or \tilde{h}/\tilde{s} , respectively. For Theory III the dark matter detection entries are a very brief summary of Figures 5, 7 and 8. The last three signals are for the far future.

theory may be similar to those of Theory II or III. Furthermore, all five theories with E-WIMP dark matter may be impossible or very difficult to probe at the LHC, other than via the value of the Higgs mass.

The Higgs mass is predicted very precisely in Theories I and II for large $\tan \beta$, and also in Theory III with $y \lesssim 0.4$. The central value is 141.0 GeV in Theory I, and just 0.54 GeV (0.35 GeV) higher in Theory II (III). In all three cases, the theoretical uncertainties are at the level of 0.4 GeV, while the experimental uncertainty of the top quark mass (QCD coupling) leads to an uncertainty in the Higgs mass of $\pm 1.8 \text{ GeV}$ ($\mp 1.0 \text{ GeV}$). In Theory III with $y \gtrsim 0.4$ the additional Yukawa interaction leads to a very significant increase in the Higgs mass, as shown in Figure 2. In Theories IV and V the Higgs mass is reduced by having a lower value of \tilde{m} and additional contributions to the gauge beta functions. The main difference between the Higgs mass prediction in Theories IV and V is that in Split Supersymmetry the Higgs boson has additional Yukawa couplings, increasing the Higgs mass; however, the amount of increase is limited because these couplings are determined by the electroweak gauge couplings and so not large. A low value of the Higgs mass is expected in Theory VI, although the tension with the experimental bound is not so tight as in the MSSM since the superpartner spectrum is less constrained. For example, an upper value of $\approx 125 \text{ GeV}$ (130 GeV) occurs for top squarks of 10 TeV with small (large) A_t .

Which observations can discriminate between these six theories, and convince us that one of them is indeed correct? For Theories I through V, can we get evidence for a very large amount of fine-tuning associated with a very high scale of supersymmetry breaking? Here we will content ourselves with a comparison of the signals of Theories I, II and III, which all have \tilde{m} of order the unification scale $M_u \sim 10^{14} \text{ GeV}$. The signals are summarized in Table 6.

The precision measurement of the Higgs mass at LHC is particularly important, since the theoretical

prediction of $\simeq (141 - 142)$ GeV is only evaded in Theory III with large y , or in Theories I and II if $\tan\beta$ is relevant. A precise measurement near 141 GeV would by itself provide significant evidence for a very high supersymmetry breaking scale, no matter what the underlying theory. If the Higgs mass lies above this special number by more than the uncertainties arising from the experimental errors in the top quark mass and QCD coupling, Theories I and II will both be excluded. A Higgs mass in the window $\simeq (127 - 142)$ GeV would be suggestive of Theory I or II, while a value above 141 GeV, but below 210 GeV, would accurately determine y in Theory III.

The indirect detection of dark matter from annihilations to $\gamma\gamma$ at the galactic center will provide a crucial measurement. A large signal at a planned atmospheric Cerenkov telescope corresponding to $\sigma v \sim 10^{-25} \text{ cm}^3\text{s}^{-1}$ and $E_\gamma \simeq 3$ TeV, when combined with a Higgs mass measurement in the window $(127 - 142)$ GeV, would provide strong evidence for Theory II. This would be compelling for a Higgs mass at the upper end of the window, implying ~ 24 orders of magnitude fine-tuning. For Theory III, Figure 8 shows that, for a wide range of dark matter masses, $100 \text{ GeV} \lesssim m_{\text{DM}} \lesssim 1 \text{ TeV}$, a monochromatic photon signal from the galactic center should be seen with $\sigma v \gtrsim 10^{-30} \text{ cm}^3\text{s}^{-1}$. Except for very small regions of parameter space at low m_{DM} and low y , a smaller value of σv only occurs at large y , and this must be correlated with a heavy Higgs. Thus the combination of the Higgs mass and monochromatic photon measurements serves to essentially distinguish the three theories.

Further discrimination between the theories is provided by direct detection of dark matter. Figure 7 shows that in Theory III with $m_{\text{DM}} < 800$ GeV a signal with $\sigma v \sim (10^{-9} - 10^{-7})$ pb is expected for any value of y . While none of the signal region is presently excluded, much is within reach of XENON 100kg and LUX 300kg. Theory II predicts $\sigma_{\text{SI}}^p \simeq 2 \times 10^{-9}$ pb and, since $m_{\text{DM}} \simeq 3$ TeV, experiments beyond XENON 100kg and LUX 300kg will be needed.

In Theories I and II there is no possibility of any signal of new physics beyond the SM Higgs at the LHC. A trilepton signal for Theory III is possible, and the most favorable region of parameter space is low μ and m and also low y . However, with an integrated luminosity of 100 fb^{-1} , the number of signal events is at most of order 100, and the background is about a factor 3 larger, so that even in this favorable case it is not clear that y can be extracted sufficiently accurately to allow a precise correlation with the Higgs mass. For Theory III a precise determination of parameters via the Higgsino/singlino masses and couplings would require a linear e^+e^- collider. If the dark matter mass is approaching 1 TeV, a muon collider may be more effective.

While a Higgs mass near 141 GeV would point towards Theory I, it would become convincing only after excluding Theories II and III. The absence of an indirect detection γ signal with $\sigma v > 10^{-26} \text{ cm}^3\text{s}^{-1}$ at 3 TeV would clearly exclude Theory II. For Theory III, the absence of a direct detection signal with $\sigma v > 10^{-9}$ pb would essentially exclude $100 \text{ GeV} \lesssim m_{\text{DM}} \lesssim 800 \text{ GeV}$. Theory III with $m_{\text{DM}} \gtrsim 800 \text{ GeV}$, the case of dominant Higgsino dark matter, would be excluded by the absence of an indirect γ signal with $\sigma v > 10^{-29} \text{ cm}^3\text{s}^{-1}$, while that with $m_{\text{DM}} \lesssim 100 \text{ GeV}$ may be within the reach of the LHC.

The main theoretical motivation for the LHC is to uncover the physics behind the weak scale by discovering new particles beyond the SM. However, this motivation assumes that the weak scale is naturally related to some other mass scale, such as the scale of some new strong force or of supersymmetry breaking, without any fine-tuning. If the weak scale arises from environmental selection on a multiverse, the most significant evidence from the LHC may lie in the value of the Higgs boson mass. Combining this with results from the direct and indirect detection of galactic dark matter could convincingly uncover the nature of the weak scale theory, providing strong evidence for both the multiverse and supersymmetry at unified scales.

Acknowledgments

P.K. thanks Hitoshi Murayama and Tomer Volansky for useful discussions. This work was supported in part by the Director, Office of Science, Office of High Energy and Nuclear Physics, of the US Department of Energy under Contract DE-AC02-05CH11231, and in part by the National Science Foundation under grants PHY-0457315, PHY-0555661 and PHY-0855653.

References

- [1] S. Perlmutter *et al.* [Supernova Cosmology Project Collaboration], *Astrophys. J.* **517**, 565 (1999) [arXiv:astro-ph/9812133]; A. G. Riess *et al.* [Supernova Search Team Collaboration], *Astron. J.* **116**, 1009 (1998) [arXiv:astro-ph/9805201].
- [2] E. Komatsu *et al.* [WMAP Collaboration], *Astrophys. J. Suppl.* **180**, 330 (2009) [arXiv:0803.0547 [astro-ph]]; M. Kowalski *et al.* [Supernova Cosmology Project Collaboration], *Astrophys. J.* **686**, 749 (2008) [arXiv:0804.4142 [astro-ph]].
- [3] S. Weinberg, *Phys. Rev. Lett.* **59**, 2607 (1987).
- [4] V. Agrawal, S. M. Barr, J. F. Donoghue and D. Seckel, *Phys. Rev. D* **57**, 5480 (1998) [arXiv:hep-ph/9707380]; T. Damour and J. F. Donoghue, *Phys. Rev. D* **78**, 014014 (2008) [arXiv:0712.2968 [hep-ph]].
- [5] R. Bousso and J. Polchinski, *JHEP* **06**, 006 (2000) [arXiv:hep-th/0004134]; S. Kachru, R. Kallosh, A. Linde and S. P. Trivedi, *Phys. Rev. D* **68**, 046005 (2003) [arXiv:hep-th/0301240]; L. Susskind, arXiv:hep-th/0302219; M. R. Douglas, *JHEP* **05**, 046 (2003) [arXiv:hep-th/0303194].
- [6] For recent discussions on environmental selection for dark matter, see, e.g., M. Tegmark, A. Aguirre, M. J. Rees and F. Wilczek, *Phys. Rev. D* **73**, 023505 (2006) [arXiv:astro-ph/0511774]; S. Hellerman and J. Walcher, *Phys. Rev. D* **72**, 123520 (2005) [arXiv:hep-th/0508161].
- [7] N. Arkani-Hamed and S. Dimopoulos, *JHEP* **0506**, 073 (2005) [arXiv:hep-th/0405159]; G. F. Giudice and A. Romanino, *Nucl. Phys. B* **699**, 65 (2004) [Erratum-ibid. B **706**, 65 (2005)] [arXiv:hep-ph/0406088]; N. Arkani-Hamed, S. Dimopoulos, G. F. Giudice and A. Romanino, *Nucl. Phys. B* **709**, 3 (2005) [arXiv:hep-ph/0409232].
- [8] N. Arkani-Hamed, S. Dimopoulos and S. Kachru, arXiv:hep-th/0501082.
- [9] R. Mahbubani and L. Senatore, *Phys. Rev. D* **73**, 043510 (2006) [arXiv:hep-ph/0510064].
- [10] L. J. Hall and Y. Nomura, *Phys. Rev. D* **64**, 055003 (2001) [arXiv:hep-ph/0103125].
- [11] L. J. Hall and Y. Nomura, *Phys. Rev. D* **65**, 125012 (2002) [arXiv:hep-ph/0111068].
- [12] L. J. Hall and Y. Nomura, arXiv:0910.2235 [hep-ph].
- [13] The Tevatron Electroweak Working Group, arXiv:0903.2503 [hep-ex].

- [14] C. Amsler *et al.* [Particle Data Group], Phys. Lett. B **667**, 1 (2008), and 2009 partial update for the 2010 edition.
- [15] G. Belanger, F. Boudjema, A. Pukhov and A. Semenov, Comput. Phys. Commun. **177**, 894 (2007).
- [16] E. Komatsu *et al.* [WMAP Collaboration], in Ref. [2].
- [17] J. Hisano, S. Matsumoto, M. Nagai, O. Saito and M. Senami, Phys. Lett. B **646**, 34 (2007) [arXiv:hep-ph/0610249].
- [18] CDFNote-9713
- [19] The TEVNPH Collaboration, arXiv:0911.3930 [hep-ex].
- [20] S. Abdullin *et al.*, Eur. Phys. J. C **39S2**, 41 (2005).
- [21] G. L. Bayatian *et al.* [CMS Collaboration], J. Phys. G **34**, 995 (2007).
- [22] ATLAS detector and physics performance. Technical design report. Vol. 2.
- [23] R. Enberg, P. J. Fox, L. J. Hall, A. Y. Papaioannou and M. Papucci, JHEP **0711**, 014 (2007) [arXiv:0706.0918 [hep-ph]].
- [24] G. Aad *et al.* [The ATLAS Collaboration], arXiv:0901.0512 [hep-ex].
- [25] W. Vandelli, CERN-THESIS-2007-072.
- [26] J. Hisano, S. Matsumoto, M. M. Nojiri and O. Saito, Phys. Rev. D **71**, 015007 (2005) [arXiv:hep-ph/0407168].
- [27] R. Gaitskell and J. Filippini, <http://dendera.berkeley.edu/plotter/entryform.html>, and references therein.
- [28] C.-L. Shan, New J. Phys. **11**, 105013 (2009) [arXiv:0903.4320 [hep-ph]].
- [29] M. Drees and C.-L. Shan, JCAP **0806**, 012 (2008) [arXiv:0803.4477 [hep-ph]].
- [30] A. M. Green, JCAP **0807**, 005 (2008) [arXiv:0805.1704 [hep-ph]].
- [31] L. Bergström, P. Ullio and J. H. Buckley, Astropart. Phys. **9**, 137 (1998) [arXiv:astro-ph/9712318].
- [32] J. Hisano, S. Matsumoto and M. M. Nojiri, Phys. Rev. Lett. **92**, 031303 (2004) [arXiv:hep-ph/0307216]; J. Hisano, S. Matsumoto, M. M. Nojiri and O. Saito, Phys. Rev. D **71**, 063528 (2005) [arXiv:hep-ph/0412403].
- [33] J. Buckley *et al.*, arXiv:0810.0444 [astro-ph]; <http://www.cta-observatory.org>
- [34] A. Arvanitaki and P. W. Graham, Phys. Rev. D **72**, 055010 (2005) [arXiv:hep-ph/0411376].
- [35] E. A. Baltz *et al.*, JCAP **0807**, 013 (2008) [arXiv:0806.2911 [astro-ph]].
- [36] F. Aharonian *et al.* [H.E.S.S. Collaboration], Phys. Rev. Lett. **97**, 221102 (2006) [Erratum-ibid. **97**, 249901 (2006)] [arXiv:astro-ph/0610509].

- [37] P. D. Serpico and G. Zaharijas, *Astropart. Phys.* **29**, 380 (2008) [arXiv:0802.3245 [astro-ph]].
- [38] G. Bertone and D. Merritt, *Phys. Rev. D* **72**, 103502 (2005) [arXiv:astro-ph/0501555].
- [39] G. Bertone, C. B. Jackson, G. Shaughnessy, T. M. P. Tait and A. Vallinotto, *Phys. Rev. D* **80**, 023512 (2009) [arXiv:0904.1442 [astro-ph.HE]].
- [40] D. M. Pierce, J. A. Bagger, K. T. Matchev and R.-J. Zhang, *Nucl. Phys. B* **491**, 3 (1997) [arXiv:hep-ph/9606211]; H.-C. Cheng, B. A. Dobrescu and K. T. Matchev, *Nucl. Phys. B* **543**, 47 (1999) [arXiv:hep-ph/9811316].
- [41] R. Essig, *Phys. Rev. D* **78**, 015004 (2008) [arXiv:0710.1668 [hep-ph]]; M. Cirelli and A. Strumia, *New J. Phys.* **11**, 105005 (2009) [arXiv:0903.3381 [hep-ph]].
- [42] R. Barate *et al.* [ALEPH Collaboration], *Phys. Lett. B* **565**, 61 (2003) [arXiv:hep-ex/0306033]; LEP Higgs Working Group Collaboration, arXiv:hep-ex/0107030.
- [43] A. D. Linde, *Phys. Lett. B* **201**, 437 (1988); F. Wilczek, arXiv:hep-ph/0408167; M. Tegmark, A. Aguirre, M. J. Rees and F. Wilczek, in Ref. [6].
- [44] A. Arvanitaki, C. Davis, P. W. Graham, A. Pierce and J. G. Wacker, *Phys. Rev. D* **72**, 075011 (2005) [arXiv:hep-ph/0504210].
- [45] P. W. Graham and S. Rajendran, arXiv:0906.4657 [hep-ph].